Superheavy nuclei in a microscopic collective Hamiltonian approach: The impact of beyond-mean-field correlations on ground state and fission properties

Z. Shi,[1] A. V. Afanasjev,[2,3] Z. P. Li,[4] and J. Meng[5,3]

[1]*School of Physics and Nuclear Energy Engineering, Beihang University, Beijing 100191, China*
[2]*Department of Physics and Astronomy, Mississippi State University, Mississippi 39762, USA*
[3]*Yukawa Institute for Theoretical Physics, Kyoto University, Kyoto 606-8502, Japan*
[4]*School of Physical Science and Technology, Southwest University, Chongqing 400715, China*
[5]*State Key Laboratory of Nuclear Physics and Technology, School of Physics, Peking University, Beijing 100871, China*

(Received 26 December 2018; published 12 June 2019)

The impact of beyond-mean-field effects on the ground state and fission properties of superheavy nuclei has been investigated in a five-dimensional collective Hamiltonian based on covariant density functional theory. The inclusion of dynamical correlations reduces the impact of the $Z = 120$ shell closure and induces substantial collectivity for the majority of the $Z = 120$ nuclei which otherwise are spherical at the mean-field level (as seen in the calculations with the PC-PK1 functional). Thus, they lead to a substantial convergence of the predictions of the functionals DD-PC1 and PC-PK1 which are different at the mean-field level. On the contrary, the predictions of these two functionals remain distinctly different for the $N = 184$ nuclei even when dynamical correlations are included. These nuclei are mostly spherical (oblate) in the calculations with PC-PK1 (DD-PC1). Our calculations for the first time reveal significant impact of dynamical correlations on the heights of inner fission barriers of superheavy nuclei with soft potential energy surfaces, the minimum of which at the mean-field level is located at spherical shape. These correlations affect the fission barriers of the nuclei, which are deformed in the ground state at the mean-field level, to a lesser degree.

DOI: 10.1103/PhysRevC.99.064316

I. INTRODUCTION

One of the most active subfields of low-energy nuclear physics is the investigation of superheavy elements (SHE) [1]. At present, the nuclear chart extends up to the element Og with proton number $Z = 118$ [2]. However, the experimental difficulties in the studies of SHEs at this extreme of the proton number are enormous: the experiments lasting several months typically provide only few events [1]. New facilities such as Superheavy Element Factory in Dubna, Russia [3] will allow to observe substantially more events at presently available Z values and hopefully to extend the nuclear chart to higher Z values.

In addition to experimental challenges, there are substantial theoretical uncertainties related to the predictions of the position of the center of the island of stability of superheavy elements [4–7] and their fission properties [8,9]. Different models locate this center at different particle numbers. For example, the microscopic+macroscopic (MM) models put it at $Z = 114, N = 184$ [4,10,11]. Most of the Skyrme energy density functionals (SEDF) place it at $Z = 126, N = 184$ [5,6]. However, there are also some SEDFs which predict large shell gap at $Z = 120$ [5].

Note that the number of these predictions was obtained in the calculations restricted to spherical shape. The danger of this restriction has recently been illustrated in the covariant density functional theoretical (CDFT [12–14]) study of Ref. [7] based on axial relativistic Hartree-Bogoliubov (RHB) calculations. Earlier CDFT studies [5,6,15–17] restricted to spherical shape almost always indicated $Z = 120, N = 172$ as the center of the island of stability of SHEs. However, the inclusion of deformation has drastically changed this situation: it was found that the impact of the $N = 172$ spherical shell gap on the structure of SHE is very limited. Similar to nonrelativistic functionals, some covariant functionals predict the important role played by the spherical $N = 184$ gap. For these functionals (NL3* [18], DD-ME2 [19], and PC-PK1 [20]) there is a band of spherical nuclei along and near the $Z = 120$ and $N = 184$ lines. However, for other functionals (DD-PC1 [22] and DD-MEδ [21]) oblate shapes dominate at and in the vicinity of these lines. Available experimental data (which do not extend up to the $Z = 120$ and $N = 184$ lines) are described with comparable accuracy in the calculations with these functionals which does not allow to discriminate between these predictions. Note that all these functionals are globally tested [7,9,23] and only DD-MEδ is not recommended for the nuclei beyond lead region based on the studies of inner fission barriers [9] and octupole deformed nuclei [24].

The results obtained in Ref. [7] on the structure of the ground states of superheavy nuclei could be further modified. This is because the potential energy surfaces of many nuclei along the $Z = 120$ and $N = 184$ lines are soft in quadrupole deformation (see Figs. 3 and 4 of Ref. [7] and Fig. 1 in the present manuscript). For such transitional nuclei the correlations beyond mean field may substantially modify the physical situation, for example, by creating deformed ground state instead of spherical one at the mean-field level. However, this issue has not been investigated before since the studies of

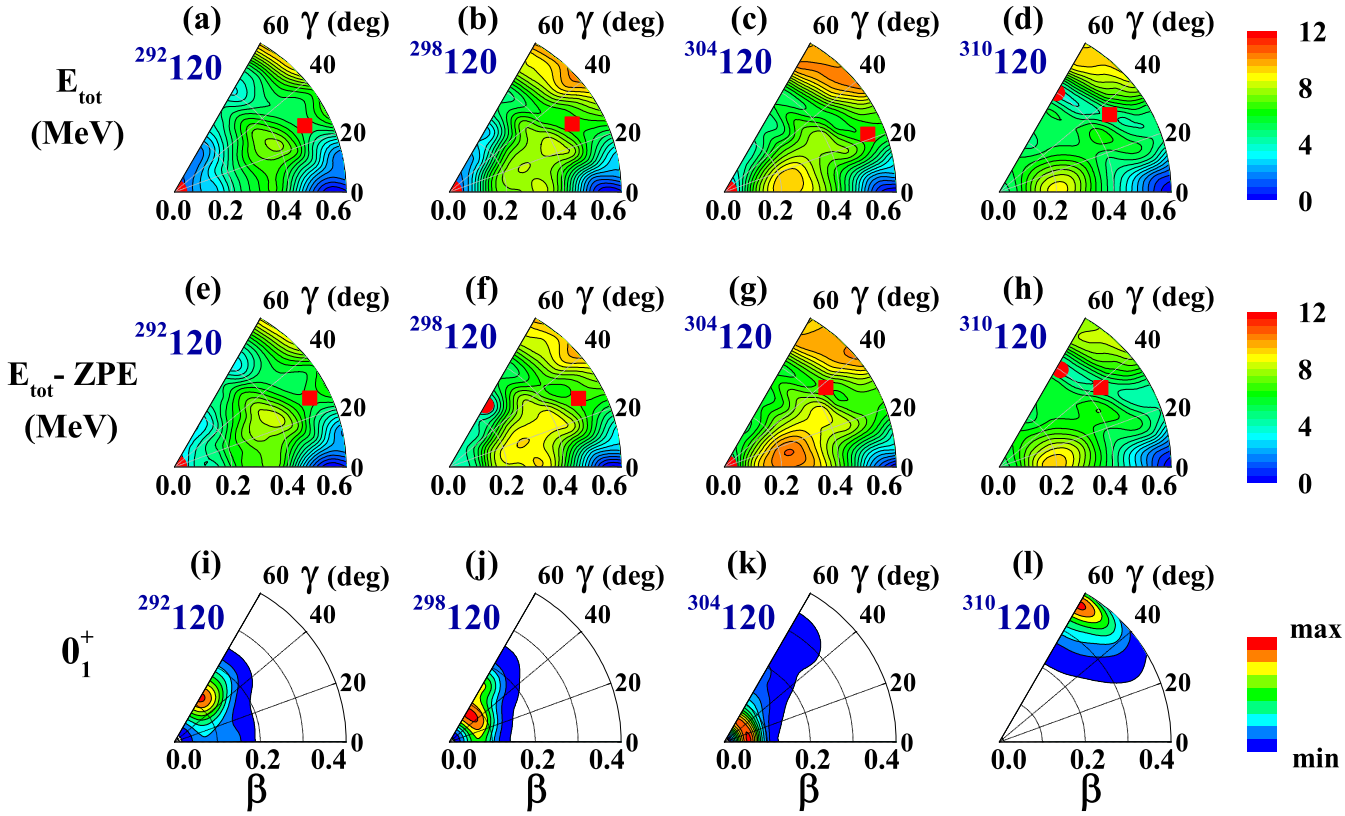

FIG. 1. Potential energy surfaces (top panels), collective energy surfaces (CES) with zero-point-energy (ZPE) taken into account (middle panels), and probability density distributions (in arbitrary units) in the β-γ plane for the 0_1^+ states (bottom panels) of selected nuclei in $Z = 120$ isotopic chain. The results are obtained with PC-PK1 CEDF. The energy difference between two neighboring equipotential lines is equal to 0.5 MeV. The minima and saddles in top and middle panels are shown by circles and squares, respectively.

SHEs are almost always done on the mean-field level. Only in Ref. [25] the beyond-mean-field effects have been taken into account for the ground states of several SHE located in the α-decay chains of the $^{298,300}120$ nuclei in the relativistic calculations based on the DD-PC1 functional.

Another question of interest is the impact of dynamical correlations on the fission barrier heights. So far the majority of the fission barrier calculations have been performed at the mean-field level (see Refs. [8,9,26–29] and references therein). Substantial differences in the predictions of inner fission barrier heights for SHE existing between different nonrelativistic and relativistic models and between different covariant energy density functionals in the CDFT calculations are summarized in Figs. 12 and 10 of Ref. [9], respectively. The CDFT predictions for the inner fission barrier heights of SHE are located at the lower end of the range of predictions of all considered models/functionals in these figures.

The importance of dynamical correlations in triaxial calculations has been studied only for few actinide [30–33] and light superheavy [34] nuclei. However, the impact of dynamical correlations on fission barriers of SHE has not been studied in a relativistic framework. Contrary to the actinides in which the ground state is prolate deformed, the situation for superheavy nuclei in the vicinity of the $Z = 120$ and $N = 184$ lines is different since such nuclei have either spherical or oblate deformation in the ground state and are transitional in nature [7]. Considering significant impact of the fission barriers on the stability of superheavy nuclei, it is necessary to evaluate the impact of dynamical correlations on their heights.

The present manuscript aims at the investigation of the impact of dynamical correlations on the ground state and fission properties of superheavy nuclei along the $Z = 120$ isotopic chain (with $N = 172 - 190$), $N = 174$ (with $Z = 108 - 124$), and $N = 184$ (with $Z = 112 - 122$) isotonic chains. The calculations are performed within five-dimensional collective Hamiltonian (5DCH) approach [35–37] based on CDFT which has been extremely successful in the description of many physical phenomena [39–46].

They are carried out with two covariant energy density functionals (CEDFs), namely, PC-PK1 [20] and DD-PC1 [22], representing two extremes of the predictions for superheavy nuclei in the CDFT. PC-PK1 predicts the bands of spherical nuclei along $Z = 120$ and $N = 184$ [7] suggesting that the $^{304}120$ nucleus may be considered as doubly magic. On the contrary, the nuclei along these lines and beyond are oblate in the calculations with DD-PC1 [7]. Note that these two functionals provide the best description of experimental data in actinides and superheavy nuclei among five employed in Ref. [7] state-of-the-art CEDFs.

In Sec. II we present a short outline of theoretical framework for the 5DCH approach based on CDFT. The systematics of collective potential energy surfaces, deformations, low-energy spectra, and fission barriers are discussed in Sec. III. Section IV summarizes the principal results.

II. THEORETICAL FRAMEWORK

The 5DCH that describes the nuclear excitations of quadrupole vibration and rotation is expressed in terms of two deformation parameters β and γ and three Euler angles $(\phi, \theta, \psi) \equiv \Omega$ [35–37],

$$\hat{H}_{\rm coll}(\beta,\gamma,\Omega) = \hat{T}_{\rm vib}(\beta,\gamma) + \hat{T}_{\rm rot}(\beta,\gamma,\Omega) + V_{\rm coll}(\beta,\gamma). \tag{1}$$

The three terms in $\hat{H}_{\rm coll}(\beta,\gamma,\Omega)$ are the vibrational kinetic energy

$$\begin{aligned}\hat{T}_{\rm vib} = -\frac{\hbar^2}{2\sqrt{wr}}\Bigg\{&\frac{1}{\beta^4}\left[\frac{\partial}{\partial\beta}\sqrt{\frac{r}{w}}\beta^4 B_{\gamma\gamma}\frac{\partial}{\partial\beta} - \frac{\partial}{\partial\beta}\sqrt{\frac{r}{w}}\beta^3 B_{\beta\gamma}\frac{\partial}{\partial\gamma}\right]\\ &+\frac{1}{\beta\sin 3\gamma}\left[-\frac{\partial}{\partial\gamma}\sqrt{\frac{r}{w}}\sin 3\gamma B_{\beta\gamma}\frac{\partial}{\partial\beta}\right.\\ &\left.+\frac{1}{\beta}\frac{\partial}{\partial\gamma}\sqrt{\frac{r}{w}}\sin 3\gamma B_{\beta\beta}\frac{\partial}{\partial\gamma}\right]\Bigg\},\end{aligned} \tag{2}$$

the rotational kinetic energy

$$\hat{T}_{\rm rot} = \frac{1}{2}\sum_{k=1}^{3}\frac{\hat{J}_k^2}{\mathcal{I}_k}, \tag{3}$$

and the collective potential $V_{\rm coll}$, respectively. Here, $\hat{J}_k$ denote the components of the total angular momentum in the body-fixed frame, and both the mass parameters $B_{\beta\beta}$, $B_{\beta\gamma}$, $B_{\gamma\gamma}$ and the moments of inertia $\mathcal{I}_k$ depend on the quadrupole deformation variables β and γ. Two additional quantities that appear in the $\hat{T}_{\rm vib}$ term, $r = B_1B_2B_3$ and $w = B_{\beta\beta}B_{\gamma\gamma} - B_{\beta\gamma}^2$, determine the volume element in the collective space.

The eigenvalue problem of the Hamiltonian Eq. (1) is solved using an expansion of eigenfunctions in terms of a complete set of basis functions that depend on five collective coordinates β, γ and $\Omega(\phi,\theta,\psi)$ [36]. The eigenfunctions of the collective Hamiltonian read as

$$\Psi_\alpha^{IM}(\beta,\gamma,\Omega) = \sum_{K\in\Delta I}\psi_{\alpha K}^I(\beta,\gamma)\Phi_{MK}^I(\Omega), \tag{4}$$

For a given collective state, the probability density distribution in the (β,γ) plane is defined as

$$\rho_{I\alpha}(\beta,\gamma) = \sum_{K\in\Delta I}\left|\psi_{\alpha K}^I(\beta,\gamma)\right|^2\beta^3, \tag{5}$$

with the summation over the allowed set of values of the projection K of the angular momentum I on the body-fixed symmetry axis, and with the normalization

$$\int_0^\infty \beta d\beta\int_0^{2\pi}\rho_{I\alpha}(\beta,\gamma)|\sin 3\gamma|d\gamma = 1. \tag{6}$$

The reduced $E2$ transition probabilities are calculated by

$$\begin{aligned}B(E2;\alpha I\to\alpha' I') &= \sum_{\mu,M',M}|\langle\alpha' I' M'|\hat{M}(E2,\mu)|\alpha I M\rangle|^2\\ &= \frac{1}{2I+1}|\langle\alpha' I'||\hat{M}(E2)||\alpha I\rangle|^2,\end{aligned} \tag{7}$$

where $\hat{M}(E2,\mu)$ is the electric quadrupole operator which can be expressed in the following form [38]:

$$\hat{M}(E2,\mu) = D_{\mu0}^2 q_{20}^p(\beta,\gamma) + \frac{1}{\sqrt{2}}\left(D_{\mu2}^2 + D_{\mu-2}^2\right)q_{22}^p(\beta,\gamma), \tag{8}$$

where

$$q_{2\kappa}^p = \left\langle\sum_p e_p r_p^2 Y_{2\kappa}\right\rangle \tag{9}$$

are the quadrupole moments for protons at the deformation point (β,γ) calculated in a fully self-consistent manner, the indices k equal to 0 and 2 and e_p are the bare charges.

In the framework of 5DCH-CDFT, the collective parameters of 5DCH, including the mass parameters $B_{\beta\beta}$, $B_{\beta\gamma}$, $B_{\gamma\gamma}$, the moments of inertia $\mathcal{I}_k$, and the collective potential $V_{\rm coll}$, are all determined microscopically from constrained triaxial CDFT calculations. The moments of inertia are calculated with Inglis-Belyaev formula [47,48] and the mass parameters with the cranking approximation [36,49]. The collective potential $V_{\rm coll}$ is calculated by

$$V_{\rm coll}(\beta,\gamma) = E_{\rm tot}(\beta,\gamma) - \Delta V_{\rm vib}(\beta,\gamma) - \Delta V_{\rm rot}(\beta,\gamma), \tag{10}$$

where $E_{\rm tot}(\beta,\gamma)$ is the mean field total energy. $\Delta V_{\rm vib}(\beta,\gamma)$ and $\Delta V_{\rm rot}(\beta,\gamma)$ are zero-point-energy (ZPE) values of vibrational and rotational motions. The collective ZPE corresponds to a superposition of zero-point motion of individual nucleons in the single-nucleon potential. Here, the ZPE corrections are calculated in the cranking approximation [36,49].

The energy surfaces $E_{\rm tot}(\beta,\gamma)$ defined as a function of deformation parameters β and γ are described as potential energy surfaces (PES). In the present manuscript, they are extracted from the triaxial relativistic mean field +BCS (RMF+BCS) calculations. The energy surfaces $V_{\rm coll}(\beta,\gamma)$ are labeled here as collective energy surfaces (CES); in addition to $E_{\rm tot}(\beta,\gamma)$ they contain zero-point-energies of vibrational and rotational motion. The CES enter into the action integral describing the fission dynamics (see Refs. [29,50] and Eq. (13) and its discussion below). Thus, the calculations of fission fragment distributions, spontaneous fission half-lives etc depend sensitively on CES (see, for example, Refs. [51,52] and references quoted therein). In addition, the height of the fission barrier is defined as an energy difference between the saddle point and minimum of CES, namely, as $V_{\rm coll}$(saddle) − $V_{\rm coll}$(min) (see, for example, Refs. [53–55]). Note that different approaches exist for the calculations of ZPE contributions to CES and in a number of publications zero-point-energies of vibrational motion are neglected since their variation with deformation is rather modest (see, for example, Ref. [54]).

III. RESULTS AND DISCUSSION

The starting point is triaxial RMF+BCS calculations. These calculations are performed imposing constraints on the axial Q_{20} and triaxial Q_{22} mass quadrupole moments. Note, that full-scale calculations are performed on the grid that covers the quadrupole deformation range $\beta_2 = 0$–0.6 in steps of $\Delta\beta_2 = 0.05$ and γ deformation range $\gamma = 0^\circ$–60° in steps of $\Delta\gamma = 6^\circ$.

To avoid the uncertainties connected with the definition of the size of the pairing window [56], we use the separable form of the finite range Gogny pairing interaction introduced by Tian *et al.* in Ref. [57] which, in addition, is multiplied by scaling factor f (see Eq. (25) in Ref. [23]). The systematic investigation of pairing properties in the actinides [23,58] indicates that scaling factor $f = 1.0$ is appropriate for the relativistic Hartree-Bogoliubov (RHB) description of actinides and superheavy nuclei and different physical observables in these mass regions are well reproduced with such a factor [7,16,23,24,58]. However, the experience shows that this factor has to be larger in the RMF+BCS framework as compared with the RHB one [59]. Thus, for the RMF+BCS framework this factor has been defined by matching the gain of binding due to proton and neutron pairing (as compared with unpaired solution) obtained in the axial RHB calculations with $f_\nu = f_\pi = 1.0$ for the $-0.6 < \beta_2 < 0.6$ deformation range of the $^{308}120$ nucleus. This led to the following neutron and proton scaling factors for the RMF+BCS calculations: $f_\nu = 1.066$ and $f_\pi = 1.052$ for the DD-PC1 functional and $f_\nu = 1.073$ and $f_\pi = 1.058$ for the PC-PK1 CEDF.

The truncation of the basis is performed in such a way that all states belonging to the major shells up to $N_F = 18$ fermionic shells are taken into account for the Dirac spinors. This truncation of the basis provides excellent numerical accuracy for the ground state properties and sufficient numerical accuracy for the changes of fission barrier heights due to the correlations beyond mean field. This basis is also sufficient for the calculation of the $E(2_1^+)$ energies and $B(E2; 2_1^+ \to 0_1^+)$ transition probabilities. This was verified by comparing the results of the 5DCH calculations with $N_F = 18$ and $N_F = 20$ for a few nuclei; the $N_F = 18$ and $N_F = 20$ results for these observables differ marginally and cannot be discriminated on the plots presented in Figs. 3 and 4 below.

However, numerically accurate calculations of absolute values of fission barrier heights in this mass region require the fermionic basis with $N_F = 20$ (see Refs. [9,28]). However, the 5DCH calculations in such a basis are prohibitively expensive and they have to be performed at all grid points. To overcome this problem we use the fact that the dynamical contributions to fission barrier height, defined as

$$E^{\rm FB}_{\rm dyn} = [\Delta V_{\rm vib}(\beta,\gamma) + \Delta V_{\rm rot}(\beta,\gamma)]_{\rm saddle} - [\Delta V_{\rm vib}(\beta,\gamma) + \Delta V_{\rm rot}(\beta,\gamma)]_{\rm ground\,state}, \quad (11)$$

calculated with $N_F = 18$ and $N_F = 20$ differ by less than 20 keV. This clearly indicates that numerical errors in the fission barriers are dominated by the truncation errors in the mean-field part. This result is born in few detailed full-scale calculations.

Note that the topologies[1] of potential energy surfaces (PES) [collective energy surfaces (CES)] are very similar in the calculations with $N_F = 18$ and $N_F = 20$ with the deformations of the ground states and saddles being almost independent of N_F. This allows simplified approach discussed below to the calculation of the fission barriers in the RMF+BCS and RMF+BCS+ZPE calculations. First, based on PES and CES obtained in the calculations with $N_F = 18$, we define the regions close to the saddle of fission barrier and ground state. Second, for these regions, the RMF+BCS calculations are repeated with $N_F = 20$ and RMF+BCS fission barrier $E^{\rm FB}_{\rm RMF+BCS}(N_F = 20)$ is defined for $N_F = 20$. Such procedure has been used earlier in Ref. [9]. Third, the fission barrier in CES is defined as

$$E^{\rm FB}_{\rm RMF+BCS+ZPE}(N_F = 20) = E^{\rm FB}_{\rm RMF+BCS+ZPE}(N_F = 18) + [E^{\rm FB}_{\rm RMF+BCS}(N_F = 20) - E^{\rm FB}_{\rm RMF+BCS}(N_F = 18)]. \quad (12)$$

This procedure saves a lot of computational time since the $N_F = 20$ calculations are performed only on a limited part of the grid space and they are performed only at the mean-field level.

The potential energy surfaces for the $Z = 120$ isotopes with $N = 172$, 178, 184, and 190 obtained in the RMF+BCS calculations with the PC-PK1 functional are shown in Fig. 1. The minima are located at spherical shape for $N = 172$, 178, and 184 and only the $^{310}120$ nucleus has an oblate ground state with $\beta_2 \approx -0.4$. Note that PES are soft in quadrupole deformation in the vicinity of the minima. As a result, the inclusion of ZPE leads to substantial modifications in a number of nuclei. For example, the $N = 178$ nucleus is no longer spherical in its ground state since the minimum in collective energy surface is located at $\beta_2 \approx -0.25$ (see Fig. 1). In addition, the collective energy surfaces are very soft in quadrupole deformation. As a consequence, the wave function of the $^{292}120$ nucleus is localized at $\beta_2 \approx -0.15$ despite the fact the minimum in collective energy is located at spherical shape. Thus, contrary to previous mean-field studies this nucleus cannot be considered in the 5DCH calculations as "doubly magic" spherical nucleus.

Figure 2 summarizes the results for the deformations of the minima in potential and collective energy surfaces for the $Z = 120$ isotopic and $N = 174$, 184 isotonic chains obtained in the RMF+BCS and RMF+BCS+ZPE calculations with the PC-PK1 and DD-PC1 CEDFs. These surfaces as well as probability densities distributions for the 0_1^+ collective wave functions are presented in Figs. 1–18 of the Supplemental Material [61]. One can see substantial changes in equilibrium deformation of the nuclei located in transitional regions when the correlations beyond mean field are included. For example, the transition from prolate to oblate shape is triggered in the

[1]The topology of potential energy surface means the general shape of multidimensional potential energy surface in terms of minima and saddles and general connectivity that characterize such a surface [60].

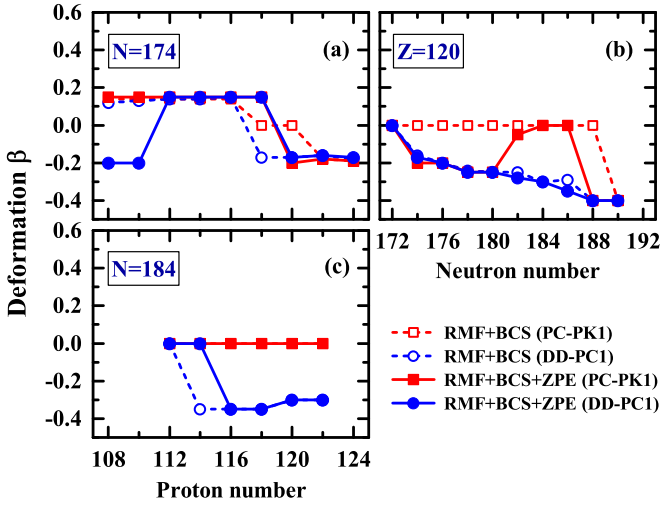

FIG. 2. The quadrupole deformations of the minima in potential and collective energy surfaces obtained in the RMF+BCS and RMF+BCS+ZPE calculations, respectively. The results obtained with DD-PC1 and PC-PK1 CEDFs are presented for the $N = 174$ (a) and $N = 184$ (c) isotonic chains as well as for the $Z = 120$ isotopic chain (b).

$N = 174$ nuclei with $Z = 108$ and 110 when ZPE are included in the calculations with DD-PC1 [Fig. 2(a)]. ZPE also triggers the transition from spherical shape to deformed one in the $N = 174$ nuclei with $Z = 118$ and 120 in the calculations with PC-PK1. The modifications are smaller in the $N = 184$ isotonic chain [Fig. 2(c)]; the deformation of the energy minimum is switched from highly deformed oblate to spherical one only in the $Z = 114$ nucleus in the calculations with DD-PC1 when ZPE are added. Otherwise, the DD-PC1 and PC-PK1 CEDF give distinctly different predictions for the deformations of the CES minima in the $N = 184$ nuclei. The former functional predicts mostly oblate shapes in the ground state, while the latter one only spherical shapes. The deformations of the $Z = 120$ nuclei are very weakly affected by the ZPE's in the calculations with DD-PC1 (Fig. 2). On the contrary, they are drastically affected by ZPE in the case of PC-PK1 CEDF; the deformations of the minima of the $N = 174$–180 and $N = 188$ isotopes change from spherical to oblate ones when ZPE is added. While the results of the RMF+BCS calculations for $Z = 120$ nuclei are drastically different for the PC-PK1 and DD-PC1, they mostly converge to the same deformed oblate solution when ZPE are added. This points to reduced role of the $Z = 120$ proton shell gap which in many earlier RMF studies was interpreted as "magic" one.

Further information on the collectivity of the states of interest can be obtained by analyzing $E(2_1^+)$ energies (Fig. 3) and the $B(E2; 2_1^+ \to 0_1^+)$ transition rates (Fig. 4). The excitation energies and transition rates are strongly affected by the quadrupole deformations of the respective minima and also by the dynamics of large shape fluctuations around equilibrium shape which strongly depends on the topology of PES. These properties can be reasonably well described in the 5DCH calculations as illustrated by the studies of the Sn isotopes in Ref. [42].

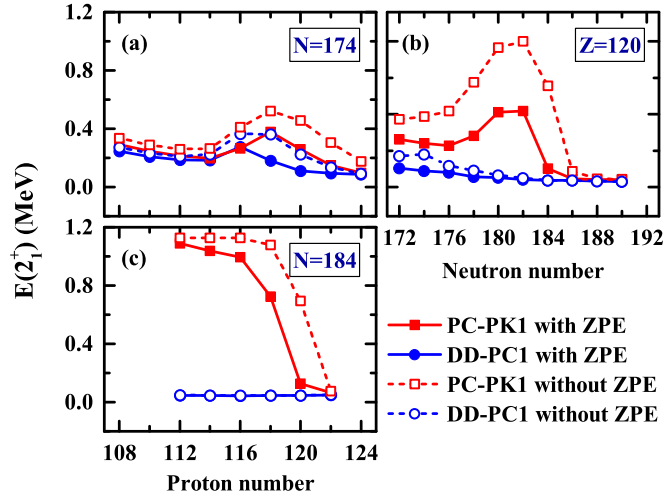

FIG. 3. Excitation energies of the 2_1^+ states a function of proton number in the $N = 174$ and 184 isotonic chains and as a function of neutron number in the $Z = 120$ isotopic chain.

With the exception of the $Z = 118$ and 120 nuclei, the results for the $E(2_1^+)$ values are very similar for the $N = 174$ isotones in the calculations with PC-PK1 and DD-PC1 CEDFs [Fig. 3(a)]. Substantial difference between the $B(E2; 2_1^+ \to 0_1^+)$ values obtained with these two functionals is observed only at $Z = 120$ [Fig. 4(a)]. Note that in this isotonic chain spherical shapes appear on the mean-field level only for the $Z = 118$ and 120 nuclei in PC-PK1 CEDF (Fig. 2); this is a reason for some weakening of the collectivity in these nuclei in the 5DCH calculations with PC-PK1 as compared with the ones based on DD-PC1 CEDF.

In the $Z = 120$ isotopic chain, the $N = 180$–184 nuclei are significantly less collective in the calculations with CEDF PC-PK1 as compared with DD-PC1 [Figs. 3(b) and 4(b)]. Above $N = 186$, there is no difference between the DD-PC1 and PC-PK1 results. Below $N = 178$, the nuclei are less

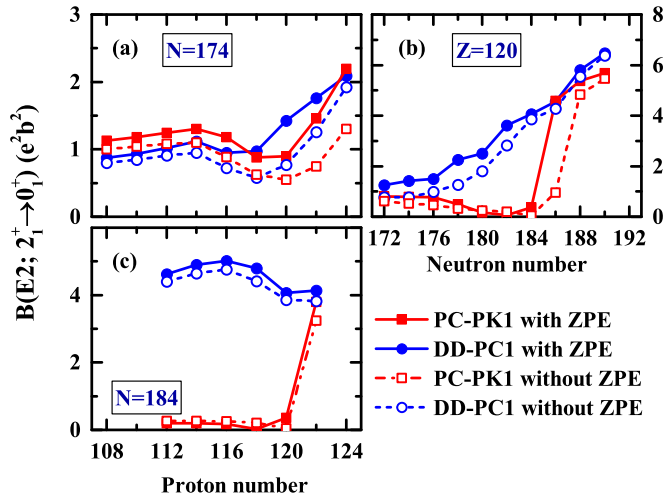

FIG. 4. The $B(E2; 2_1^+ \to 0_1^+)$ values as a function of proton number in the $N = 174$ and 184 isotonic chains and as a function of neutron number in the $Z = 120$ isotopic chain.

collective in the calculations with PC-PK1 but the difference is not that significant as in the $N = 180$–184 nuclei. All these features closely correlate with the presence/absence of spherical nuclei along the $Z = 120$ chain in the RMF+BCS calculations with PC-PK1/DD-PC1 functionals and with the modifications of PES induced by dynamical correlations [see Fig. 2(b) and Fig. 1].

The results for the $N = 184$ nuclei with $Z = 112$–118 obtained with the DD-PC1 and PC-PK1 functionals are distinctly different [Figs. 3(c) and 4(c)]. Indeed, the combination of $E(2_1^+) \approx 1.0$ MeV (which is substantially higher than the $E(2_1^+)$ values obtained for the $N = 174$ and $Z = 120$ chains) and low $B(E2; 2_1^+ \to 0_1^+)$ values obtained in the 5DCH calculations with PC-PK1 strongly suggests that the $Z = 112$–118, $N = 184$ nuclei may be considered as truly spherical. The $Z = 120, N = 184$ nucleus is transitional in nature with small $E(2_1^+)$ and $B(E2; 2_1^+ \to 0_1^+)$ values and the $Z = 122$, $N = 184$ nucleus is collective in ground state in the calculations with PC-PK1. However, all $N = 184$ isotones are collective in their ground states in the calculations with DD-PC1.

It is interesting to investigate the impact of ZPE on the $E(2_1^+)$ energies and $B(E2; 2_1^+ \to 0_1^+)$ transition rates. This is done by neglecting ZPE in the 5DCH calculations; such results are shown by dashed lines with open symbols in Figs. 3 and 4.

The neglect of ZPE typically leads to the increase of the $E(2_1^+)$ energies and there is a correlation between the magnitude of this increase and the deformation of the system. This increase is either small or even nonexistent in the results obtained with the DD-PC1 functional (see Fig. 3); note that the absolute majority of the calculated nuclei have nonzero β deformations for the ground states in the RMF+BCS and 5DCH calculations with this functional (see Fig. 2). These deformations are similar or have similar magnitude for the $N = 174$ isotopic chain in the calculations with DD-PC1 and PC-PK1 [see Fig. 2(a)]. As a result, the increase in the $E(2_1^+)$ energies due to neglect of ZPE is comparable in both functionals. On the contrary, in the calculations with PC-PK1 the increases in the $E(2_1^+)$ energies due to neglect of ZPE are larger in the $N = 184$ isotonic chain [see Fig. 3(c)] and they are especially large in the $Z = 120$ isotopic chain [see Fig. 3(b)]. In the former chain, the ground states of the nuclei have $\beta = 0$ both in the RMF+BCS and RMF+BCS+ZPE calculations [see Fig. 2(c)]. In the latter chain, with exception of the $N = 190$ nucleus, in the ground states the β deformation is zero in the RMF+BCS calculations and the inclusion of ZPE triggers the transition to oblate deformation in the nuclei with $N = 174$–180 and $N = 188$ [see Fig. 2(b)].

In general, the neglect of ZPE leads to the decrease of the $B(E2; 2_1^+ \to 0_1^+)$ transition rates (see Fig. 4). The only exceptions are the $N = 184$ nuclei with $Z = 112$–118 [see Fig. 4(c)] and $Z = 120$ nuclei with $N = 180, 182$ [see Fig. 4(b)] in the calculations with PC-PK1. However, these nuclei are characterized by very low values of $B(E2; 2_1^+ \to 0_1^+)$. Note also that the decrease of the $B(E2; 2_1^+ \to 0_1^+)$ transition rates due to the neglect of ZPE depends on the nucleus and on the functional. Note that no direct correlations between these decreases in the $B(E2; 2_1^+ \to 0_1^+)$ values and the topologies of PES and/or CES of the nuclei under consideration have been found.

Figure 5 shows the impact of dynamical correlations on the heights of inner fission barriers of the nuclei under consideration. In the mean-field calculations, the height of fission barrier is defined as the energy difference between the saddle point and minimum of PES. In the beyond-mean-field calculations, this energy difference is extracted from the energies of saddle and minimum of collective energy surface: This is consistent with the definition of fission barrier height used before in beyond-mean-field approaches based on Gogny and Skyrme energy density functionals [53–55].

The changes introduced in the fission barrier heights due to dynamical correlations are summarized in Fig. 6. The calculated heights obtained in the RMF+BCS calculations are in general close to the ones obtained in the RHB calculations of Ref. [9]; some differences are due to the use of different frameworks (RMF+BCS in the present manuscript and RHB in Ref. [9]) and the differences in the way the pairing interaction has been defined in both manuscripts. Note that the height of fission barrier extremely sensitively depends on the strengths of pairing interaction (see Ref. [56] and references quoted therein).

One can see that in the calculations with the DD-PC1 functional, the fission barriers obtained in the calculations with and without dynamical correlations are close to each other; the modifications of the fission barrier height by the dynamical correlations are typically in the range of ± 0.5 MeV (see Fig. 6). The only exceptions are the $(Z = 116, N = 174)$ [Fig. 6(a)], $(Z = 120, N = 186)$ [Fig. 6(b)], and $(Z = 116, N = 184)$ [Fig. 6(c)] nuclei for which the modifications of inner fission barrier due to dynamical correlations are close to or exceed 1 MeV. Note that the absolute majority of the nuclei under consideration are deformed in the ground states in the calculations at and beyond-mean-field levels with DD-PC1 functional (see Fig. 2 and Figs. 4, 5, 10, 11, 16, and 17 in the Supplemental Material [61]).

Similar features are also seen for the $N = 174$ isotones in the calculations with the PC-PK1 functional [see Fig. 5(d)]. The majority of the nuclei in the $N = 174$ chain are deformed both at and beyond-mean-field levels (see Fig. 6(a) and Figs. 7 and 8 in the Supplemental Material [61]) and only $Z = 118$ and 120 nuclei are spherical in the mean-field calculations. Only for the latter two nuclei the modifications of the fission barrier height by dynamical correlations are close to or exceed 1 MeV [see Fig. 6(a)].

On the contrary, substantial changes in fission barrier heights induced by dynamical correlations are seen in the nuclei which are spherical in the ground states in the RMF+BCS calculations with PC-PK1. These are the $Z = 118$, 120 nuclei in the $N = 174$ isotopic chain, the $N = 172$–182 nuclei in the $Z = 120$ chain and the $Z = 112$–116 nuclei in the $N = 184$ chain. Dynamical correlations lead to a substantial increase (decrease) of fission barriers in the $N = 184$ isotones with $Z = 112$–116 (in the $Z = 120$ isotopes with $N = 172$–182). However, they have very limited impact of the fission barriers of spherical nuclei located in close vicinity of the $Z = 120, N = 184$ nucleus; these are nuclei which have the

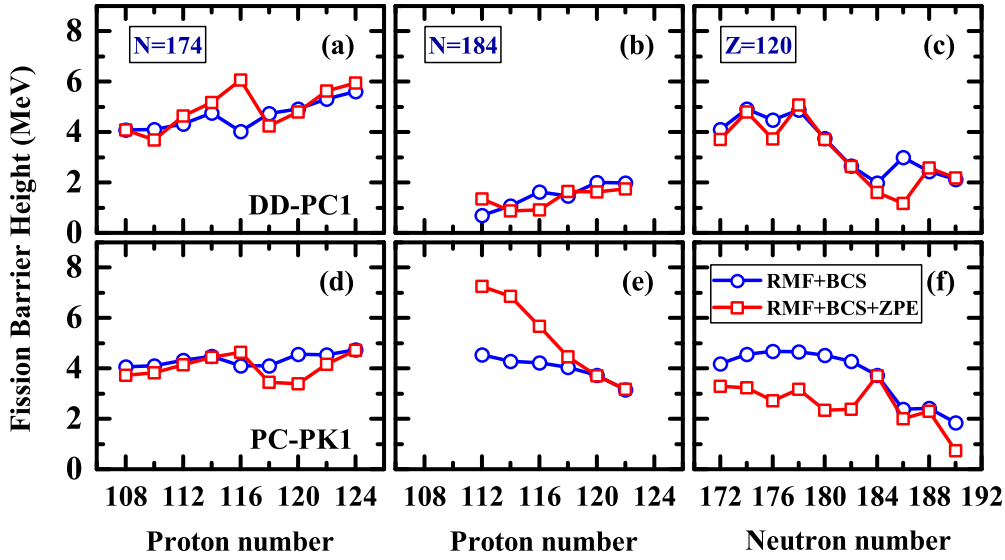

FIG. 5. The heights of inner fission barriers in the mean-field calculations (labeled as "RMF+BCS") and in the calculations with dynamical correlations included (labeled as "RMF+BCS+ZPE").

features of spherical nucleus both at and beyond-mean-field levels.

To better understand the origin of these changes in the fission barrier heights we plot dynamical correlation energies for the ground states and the saddles of inner fission barriers in Fig. 7. Several interesting features emerge from the analysis of this figure. First, the variation of dynamical correlation energies with neutron number is rather smooth at the saddles of inner fission barriers. Moreover, these energies are around of 5 MeV in all nuclei under study. On the contrary, dynamical correlation energies for the ground states typically show much larger fluctuations as a function of neutron number; these fluctuations are especially pronounced for the chains of the nuclei which are calculated to be spherical at the mean-field level. Second, these dynamical correlation energies are very similar at the ground state and the saddle of inner fission barrier in deformed nuclei [see Figs. 7(a)–7(d)]. As a consequence, the impact of dynamical correlations on the fission barriers of deformed nuclei is limited. However, they are quite different in the nuclei which have spherical ground states in the mean-field calculations. This feature explains observed increase of the importance of dynamical correlations for the calculation of inner fission barrier of SHE with soft PES the minimum of which is located at spherical shape.

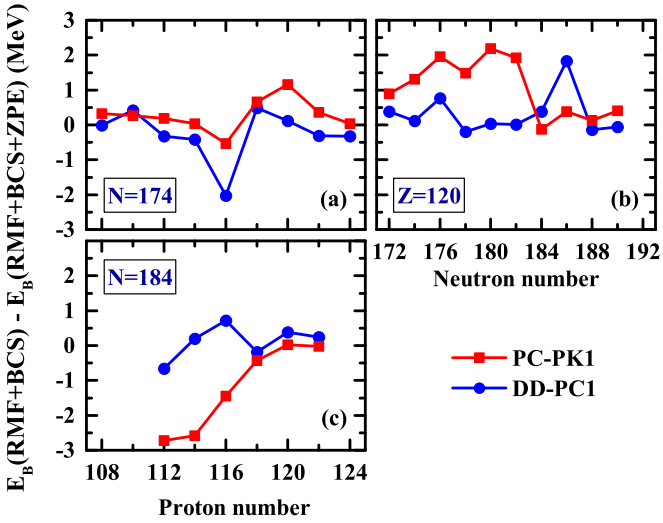

FIG. 6. The same as Fig. 2 but for the impact of dynamical correlations on the height of inner fission barrier. Negative (positive) value of E_B(RMF+BCS)-E_B(RMF+BCS+ZPE) means higher (lower) fission barrier in the calculations with dynamical correlations included.

It is also interesting to look on potential impact of the ground-state energy on the description of some fission processes. For example, the calculation of spontaneous fission half lives τ_{SF} depends on the energy E of collective ground state (see Ref. [8]) since it enters into the action integral S, corresponding to trajectory between two points **a** and **b** in **q**-space (collective coordinate space),

$$S(\mathbf{a},\mathbf{b},E)=\int_0^s \sqrt{2B_s[\mathbf{q}(s')]\{E-V[\mathbf{q}(s')]\}}ds', \qquad (13)$$

where the trajectory length counts from zero at **a** to s at **b** (see Sec. 5.1.3. in Ref. [50]). In many applications, the tunneling energy E (which is also the ground-state energy of the nucleus before fission) is either approximated by $E_0 = 0.5$ MeV (see Refs. [54,62–65]) or defined from WKB quantization rules (see Ref. [8]). In the latter case, this energy is extracted from the condition that $V(q) = E_0$ at classical turning points.

On the contrary, one can take a more microscopic approach and associate tunneling energy E with the energy of collective ground state defined either in generator coordinate method (GCM) or in 5DCH. To our knowledge, this has been done so far only in Ref. [66] in which the collective ground-state energy is defined from GCM calculations; these calculations are based on Skyrme energy density functional but are restricted

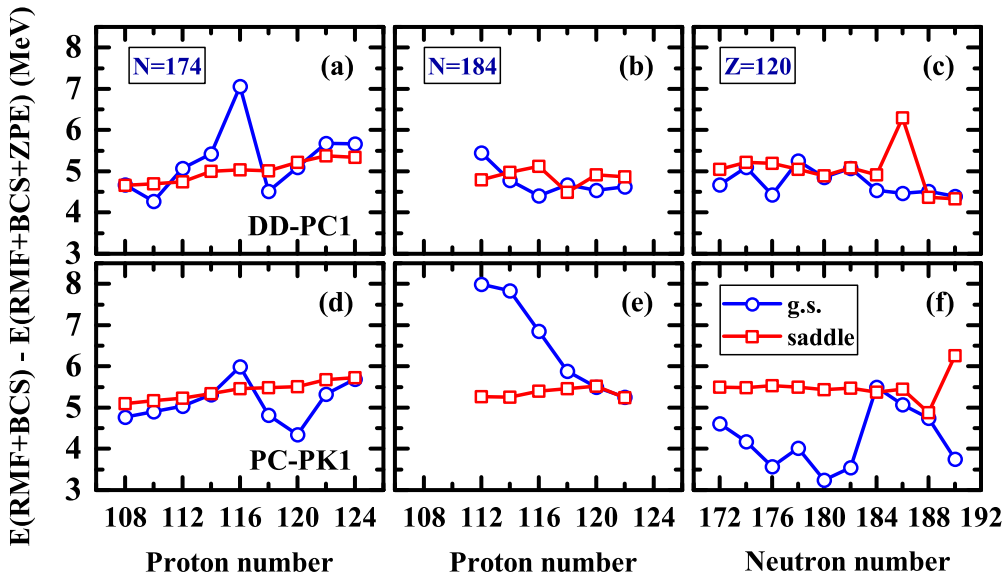

FIG. 7. Dynamical correlations energies at the ground states and the saddles of inner fission barriers of the nuclei under study.

to axial shape. As discussed in Ref. [8], the microscopic values of tunneling energies differ from approximate ones. In a similar fashion, one can associate the tunneling energy E with the energy $E(0_1^+)$ of the ground state obtained in 5DCH. The $E(0_1^+)$ energies, shown in bottom panels of Fig. 8, deviate substantially in many cases both from $E_0 = 0.5$ MeV and from the ground state energies defined by means of the WKB quantization rules (which are displayed in Fig. 4 of Ref. [8]). The differences between these values also substantially depend on proton and neutron numbers.

These differences in the values of tunneling energy E are expected to have a profound effect on spontaneous fission half lives τ_{SF}. Although the calculation of τ_{SF} is beyond the scope of the present manuscript, the comparison of $V_{coll}(\text{saddle}) - E(0_1^+)$ and $V_{coll}(\text{saddle}) - V_{coll}(\text{min})$ allows to estimate the major trends. The difference $V_{coll}(\text{saddle}) - E(0_1^+)$ defines the

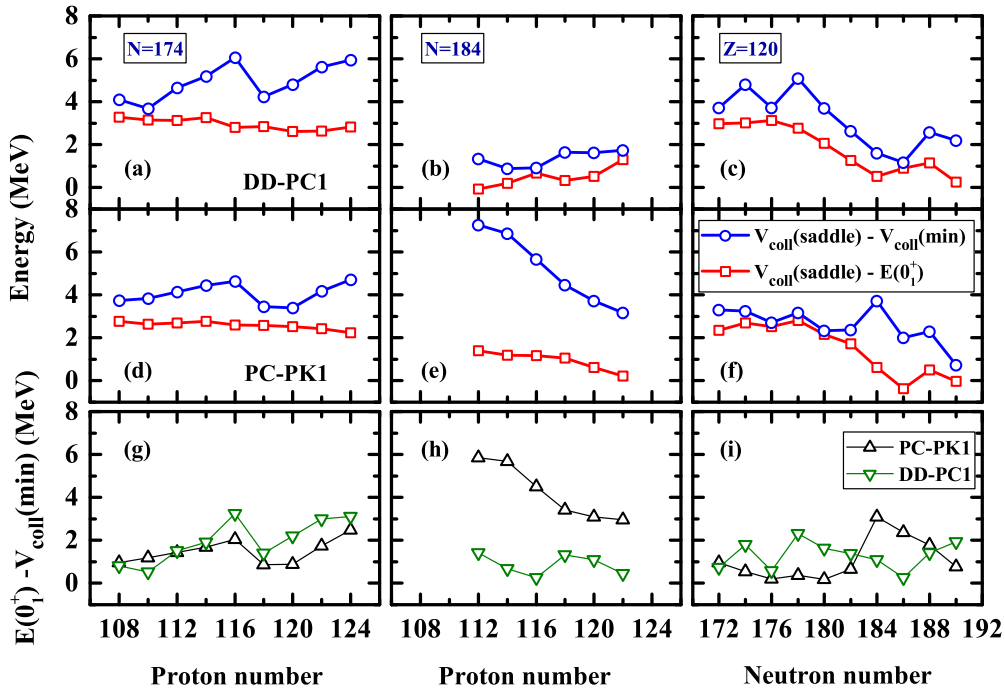

FIG. 8. The energy difference $V_{coll}(\text{saddle}) - V_{coll}(\text{min})$ between the saddle point and the minimum of collective energy surface compared with the energy difference $V_{coll} - E(0_1^+)$. The energy $E(0_1^+) - V_{coll}(\text{min})$ (shown in bottom panels) is the ground-state energy (relatively to the energy of the minimum of CES) in the 5DCH calculations.

maximum variation of the $(E - V(\mathbf{q}))$ difference in the action integral of Eq. (13). It is lower than the fission barrier height $V_{\rm coll}(\text{saddle}) - V_{\rm coll}(\text{min})$ typically by more than 0.5 MeV. In many cases this difference reaches few MeV. All this suggest that the approximation of tunneling energy by $E_0 = 0.5$ MeV (as done in many applications) is highly unreliable. The present results suggest that the use of $E(0_1^+)$ (as defined by 5DCH) for the energy of collective ground state will result in a substantial reduction of spontaneous fission half-lives as compared with estimates based on $E = E_0$.

The magnitude of the $E(0_1^+)$ with respect of the minimum of the collective energy surface [the $E(0_1^+) - V_{\rm coll}(\text{min})$ quantity in Fig. 8] depends on the softness of collective energy surface in the vicinity of spherical/normal-deformed minimum. The soft (stiff) CES leads to low (high) values of the $E(0_1^+) - V_{\rm coll}(\text{min})$ quantity. This dependence is especially pronounced in the $N = 184$ isotonic chain [see Fig. 8(h)]. The CES's of these isotopes are soft in the vicinity of spherical minimum at $Z = 112$ and oblate minimum at $Z = 114$–122 in the DD-PC1 functional (see Fig. 17 in the Supplemental Material [61]) and this leads to $E(0_1^+) - V_{\rm coll}(\text{min}) \approx 1.0$ MeV. On the contrary, the CES's are stiffer in the vicinity of spherical minimum in the PC-PK1 functional with their stiffness decreasing with increasing Z (see Fig. 14 in the Supplemental Material [61]) and this leads to substantially higher $E(0_1^+) - V_{\rm coll}(\text{min})$ values which decrease with increasing Z [see Fig. 8(h)]. Similar correlations between the softness of CES in the vicinity of the minimum under consideration and the $E(0_1^+) - V_{\rm coll}(\text{min})$ values can be found in the $Z = 120$ isotopic chain (compare Figs. 2 and 5 in the Supplemental Material [61] with Fig. 8(i) in the manuscript) and $N = 174$ isotonic chain [compare Figs. 8 and 11 in the Supplemental Material [61] with Fig. 8(g)].

IV. SUMMARY

In conclusion, the impact of beyond-mean-field effects on the ground state and fission properties of superheavy nuclei has been investigated in five-dimensional collective Hamiltonian. We focus here on two functionals (DD-PC1 and PC-PK1) which give distinctly different predictions along the $Z = 120$ and $N = 184$ lines at the mean-field level. For the first time it is shown that the inclusion of dynamical correlations brings the predictions of these two functionals closer for nuclei along the $Z = 120$ line. Only few nuclei around $N = 184$ remain spherical in the calculations with PC-PK1; the rest of nuclei possess significant collectivity. This stresses again that the impact of spherical shell closure at $Z = 120$ is quite limited. On the contrary, the predictions of these two functionals remain distinctly different for the $N = 184$ nuclei even when dynamical correlations are included. These nuclei are mostly spherical (oblate) in the calculations with PC-PK1 (DD-PC1). The impact of dynamical correlations on the height of inner fission barrier has been investigated. It is typically moderate (significant) when the ground state is deformed (spherical) at the mean-field level. This result for the first time shows the importance of the inclusion of dynamical correlations for the calculation of inner fission barriers of the superheavy nuclei with soft potential energy surfaces the minimum of which at mean-field level is located at spherical shape.

It is important to keep in mind that potential energy surfaces of many superheavy nuclei are soft also in nonrelativistic theories (see, for example, Refs. [62,67,68]). It is reasonable to expect that similar to this study the correlations beyond mean field could have a substantial impact on their ground state and fission properties and potentially on the localization and the properties of predicted islands of stability of superheavy elements.

ACKNOWLEDGMENTS

This material is based upon work supported by the US Department of Energy, Office of Science, Office of Nuclear Physics under Award No. DE-SC0013037, by the CUSTIPEN (China-US Theory Institute for Physics with Exotic Nuclei) funded by the US Department of Energy,Office of Science under Grant No. DE-SC0009971, and by the National Key R&D Program of China (Contract No. 2018YFA0404400) and the National Natural Science Foundation of China (Grants No. 11335002, No. 11475140, No. 11575148, No. 11621131001, and No. 11875225).

[1] Y. Ts. Oganessian and V. K. Utyonkov, Rep. Prog. Phys. **78**, 036301 (2015).
[2] Y. Ts. Oganessian *et al.*, Phys. Rev. Lett. **109**, 162501 (2012).
[3] Y. Ts. Oganessian and S. N. Dmitriev, Rus. Chem. Rev. **85**, 901 (2016).
[4] P. Möller and J. R. Nix, J. Phys. G **20**, 1681 (1994).
[5] M. Bender, K. Rutz, P.-G. Reinhard, J. A. Maruhn, and W. Greiner, Phys. Rev. C **60**, 034304 (1999).
[6] M. Bender, W. Nazarewicz, and P.-G. Reinhard, Phys. Lett. B **515**, 42 (2001).
[7] S. E. Agbemava, A. V. Afanasjev, T. Nakatsukasa, and P. Ring, Phys. Rev. C **92**, 054310 (2015).
[8] A. Baran, M. Kowal, P.-G. Reinhard, L. M. Robledo, A. Staszczak, and M. Warda, Nucl. Phys. A **944**, 442 (2015).
[9] S. E. Agbemava, A. V. Afanasjev, D. Ray, and P. Ring, Phys. Rev. C **95**, 054324 (2017).
[10] S. G. Nilsson, J. R. Nix, A. Sobiczewski, Z. Szymański, S. Wycech, C. Gustafson, and P. Möller, Nucl. Phys. A **115**, 545 (1968)
[11] Z. Patyk and A. Sobiczewski, Nucl. Phys. A **533**, 132 (1991).
[12] D. Vretenar, A. V. Afanasjev, G. A. Lalazissis, and P. Ring, Phys. Rep. **409**, 101 (2005).
[13] J. Meng, H. Toki, S. G. Zhou, S. Q. Zhang, W. H. Long, and L. S. Geng, Prog. Part. Nucl. Phys. **57**, 470 (2006).
[14] *Relativistic Density Functional for Nuclear Structure*, edited by J. Meng (World Scientific, Singapore), Int. Rev. Nucl. Phys. 10 (2016).

[15] K. Rutz, M. Bender, T. Bürvenich, T. Schilling, P.-G. Reinhard, J. A. Maruhn, and W. Greiner, Phys. Rev. C **56**, 238 (1997).
[16] A. V. Afanasjev, T. L. Khoo, S. Frauendorf, G. A. Lalazissis, and I. Ahmad, Phys. Rev. C **67**, 024309 (2003).
[17] W. Zhang, J. Meng, S. Q. Zhang, L. S. Geng, and H. Toki, Nucl. Phys. A **753**, 106 (2005).
[18] G. A. Lalazissis, S. Karatzikos, R. Fossion, D. Peña Arteaga, A. V. Afanasjev, and P. Ring, Phys. Lett. B **671**, 36 (2009).
[19] G. A. Lalazissis, T. Nikšić, D. Vretenar, and P. Ring, Phys. Rev. C **71**, 024312 (2005).
[20] P. W. Zhao, Z. P. Li, J. M. Yao, and J. Meng, Phys. Rev. C **82**, 054319 (2010).
[21] X. Roca-Maza, X. Viñas, M. Centelles, P. Ring, and P. Schuck, Phys. Rev. C **84**, 054309 (2011).
[22] T. Nikšić, D. Vretenar, and P. Ring, Phys. Rev. C **78**, 034318 (2008).
[23] S. E. Agbemava, A. V. Afanasjev, D. Ray, and P. Ring, Phys. Rev. C **89**, 054320 (2014).
[24] S. E. Agbemava, A. V. Afanasjev, and P. Ring, Phys. Rev. C **93**, 044304 (2016).
[25] V. Prassa, T. Nikšić, G. A. Lalazissis, and D. Vretenar, Phys. Rev. C **86**, 024317 (2012).
[26] P. Möller, A. J. Sierk, T. Ichikawa, A. Iwamoto, R. Bengtsson, H. Uhrenholt, and S. Åberg, Phys. Rev. C **79**, 064304 (2009).
[27] H. Abusara, A. V. Afanasjev, and P. Ring, Phys. Rev. C **82**, 044303 (2010).
[28] H. Abusara, A. V. Afanasjev, and P. Ring, Phys. Rev. C **85**, 024314 (2012).
[29] N. Schunck and L. M. Robledo, Rep. Prog. Phys. **79**, 116301 (2016).
[30] J. Sadhukhan, J. Dobaczweski, W. Nazarewicz, J. A. Sheikh, and A. Baran, Phys. Rev. C **90**, 061304(R) (2014).
[31] J. Zhao, B.-N. Lu, T. Nikšić, D. Vretenar, and S.-G. Zhou, Phys. Rev. C **93**, 044315 (2016).
[32] K. Benrabia, D. E. Medjadi, M. Imadalou, and P. Quentin, Phys. Rev. C **96**, 034320 (2017).
[33] J.-P. Delaroche, M. Girod, H. Goutte, and J. Libert, Nucl. Phys. A **771**, 103 (2006).
[34] R. A. Gherghescu, J. Skalski, Z. Patyk, and A. Sobiczewski, Nucl. Phys. A **651**, 237 (1999).
[35] Z. P. Li, T. Nikšić, D. Vretenar, J. Meng, G. A. Lalazissis, and P. Ring, Phys. Rev. C **79**, 054301 (2009).
[36] T. Nikšić, Z. P. Li, D. Vretenar, L. Próchniak, J. Meng, and P. Ring, Phys. Rev. C **79**, 034303 (2009).
[37] T. Nikšić, D. Vretenar, and P. Ring, Prog. Part. Nucl. Phys. **66**, 519 (2011).
[38] K. Kumar and M. Baranger, Nucl. Phys. A **92**, 608 (1967).
[39] Z. P. Li, T. Nikšić, D. Vretenar, and J. Meng, Phys. Rev. C **80**, 061301(R) (2009).
[40] Z. P. Li, T. Nikšić, D. Vretenar, P. Ring, and J. Meng, Phys. Rev. C **81**, 064321 (2010).
[41] Z. P. Li, J. M. Yao, D. Vretenar, T. Nikšić, H. Chen, and J. Meng, Phys. Rev. C **84**, 054304 (2011).
[42] Z. P. Li, C. Y. Li, J. Xiang, J. M. Yao, and J. Meng, Phys. Lett. B **717**, 470 (2012).
[43] Y. Y. Wang, Z. Shi, Q. B. Chen, S. Q. Zhang, and C. Y. Song, Phys. Rev. C **93**, 044309 (2016).
[44] S. Quan, Q. Chen, Z. P. Li, T. Nikšić, and D. Vretenar, Phys. Rev. C **95**, 054321 (2017).
[45] Z. Shi and Z. P. Li, Phys. Rev. C **97**, 034329 (2018).
[46] Z. Shi, Q. B. Chen, and S. Q. Zhang, Eur. Phys. J. A **54**, 53 (2018).
[47] D. Inglis, Phys. Rev. **103**, 1786 (1956).
[48] S. T. Beliaev, Nucl. Phys. **24**, 322 (1961).
[49] M. Girod and B. Grammaticos, Nucl. Phys. A **330**, 40 (1979).
[50] H. J. Krappe and K. Pomorski, *Theory of Nuclear Fission* (Springer-Verlag, Berlin, 2012).
[51] J. Sadhukhan, W. Nazarewicz, and N. Schunck, Phys. Rev. C **93**, 011304(R) (2016).
[52] H. Tao, J. Zhao, Z. P. Li, T. Niksic, and D. Vretenar, Phys. Rev. C **96**, 024319 (2017).
[53] J. Erler, K. Langanke, H. P. Loens, G. Martínez-Pinedo, and P.-G. Reinhard, Phys. Rev. C **85**, 025802 (2012).
[54] R. Rodríguez-Guzmán and L. M. Robledo, Phys. Rev. C **89**, 054310 (2014)
[55] S. A. Giuliani, G. Martínez-Pinedo, and L. M. Robledo, Phys. Rev. C **97**, 034323 (2018).
[56] S. Karatzikos, A. V. Afanasjev, G. A. Lalazissis, and P. Ring, Phys. Let. B **689**, 72 (2010).
[57] Y. Tian, Z. Y. Ma, and P. Ring, Phys. Let. B **676**, 44 (2009).
[58] A. V. Afanasjev and O. Abdurazakov, Phys. Rev. C **88**, 014320 (2013).
[59] J. Xiang, Z. P. Li, J. M. Yao, W. H. Long, P. Ring, and J. Meng, Phys. Rev. C **88**, 057301 (2013).
[60] O. M. Becker and M. Karplus, J. Chem. Phys. **106**, 1495 (1997).
[61] See Supplemental Material at http://link.aps.org/supplemental/10.1103/PhysRevC.99.064316 for detailed graphical information on potential energy surfaces obtained in the RMF+BCS calculations and collective energy surfaces with zero-point-energy (ZPE) taken into account for all nuclei considered in the present manuscript. It includes the locations of the ground states and saddles of inner fission barriers in the β-γ plane. In addition, the probability density distributions in the β-γ plane for the 0^+ ground states obtained in five dimensional collective Hamiltonian calculations are provided.
[62] M. Warda and J. L. Egido, Phys. Rev. C **86**, 014322 (2012).
[63] M. Warda, J. L. Egido, L. M. Robledo, and K. Pomorski, Phys. Rev. C **66**, 014310 (2002).
[64] A. Baran, Z. Lojewski, K. Sieja, and M. Kowal, Phys. Rev. C **72**, 044310 (2005).
[65] S. G. Nilsson, C. F. Tsang, A. Sobiczewski, Z. Szymański, S. Wycech, Ch. Gustafson, I.-L. Lamm, P. Möller, and B. Nilsson, Nucl. Phys. A **131**, 1 (1969).
[66] N. Schindzielorz, J. Erler, P. Klupfel, P. G. Reinhard, and G. Hager, Int. J. Mod. Phys. E **18**, 773 (2009).
[67] S. Ćwiok, P.-H. Heenen, and W. Nazarewicz, Nature **433**, 705 (2005).
[68] P. Jachimowicz, M. Kowal, and J. Skalski, Phys. Rev. C **83**, 054302 (2011).